NAVAL POSTGRADUATE SCHOOL
MONTEREY, CALIFORNIA

THESIS

BUBBLE INJECTION UNDER BREAKING WAVES

by

James B. Tannahill

December 1996

Co-Advisor: Edward B. Thornton
Co-Advisor: Timothy P. Stanton

Approved for public release; distribution is unlimited.

REPORT DOCUMENTATION PAGE

Form Approved
OMB No. 0704-0188

1. AGENCY USE ONLY (Leave Blank)	2. REPORT DATE	3. REPORT TYPE AND DATES COVERED
	December 1996	Master's Thesis

4. TITLE AND SUBTITLE
BUBBLE INJECTION UNDER BREAKING WAVES

5. FUNDING NUMBERS

6. AUTHOR(S)
Tannahill, James B.

7. PERFORMING ORGANIZATION NAME(S) AND ADDRESS(ES)
Naval Postgraduate School
Monterey, CA 93943-5000

8. PERFORMING ORGANIZATION REPORT NUMBER

9. SPONSORING / MONITORING AGENCY NAME(S) AND ADDRESS(ES)

10. SPONSORING / MONITORING AGENCY REPORT NUMBER

11. SUPPLEMENTARY NOTES
The views expressed in this thesis are those of the author and do not reflect the official policy or position of the Department of Defense or the U.S. Government.

12a. DISTRIBUTION / AVAILABILITY STATEMENT
Approved for public release, distribution is unlimited

12b. DISTRIBUTION CODE

13. ABSTRACT (Maximum 200 words)

Wave energy dissipation due to bubble penetration and inferred turbulent penetration from breaking waves in the surf zone is related to the total energy of dissipation. Bubble injection is inferred from void fraction measurements obtained using a 2.3 meter vertical array of eight conductivity sensors extending from the bottom through the water surface. Potential energy and dissipation associated with bubble injection are calculated and compared with total wave dissipation. Total wave dissipation is calculated from the energy flux balance measured using an array of seven pressure sensors in the surf zone.

Percent of total wave potential energy of the bubbles due to spilling breakers is on the order of 0.18% to 0.62%, consistent with past measurements in the surf zone. Percent of the bubble potential energy dissipation rates to total wave dissipation in the cross shore direction is on the order of 8% to 20%. The potential energy dissipation is largest immediately after injection, decaying exponentially after that. Bubble potential energy dissipation results within 1.2 seconds even for void fraction events greater than 36% and usually in less than 1.0 seconds. Energy dissipation was found linearly related (0.95 correlation coefficient) with the ratios of wave height to water depth, a measure of the percent of breaking waves within the surf zone.

14. SUBJECT TERMS	15. NUMBER OF PAGES
Bubble Injection, Void Fraction, Energy Dissipation, Wave Transformation	56
	16. PRICE CODE

17. SECURITY CLASSIFICATION OF REPORT	18. SECURITY CLASSIFICATION OF THIS PAGE	19. SECURITY CLASSIFICATION OF ABSTRACT	20. LIMITATION OF ABSTRACT
Unclassified	Unclassified	Unclassified	UL

NSN 7540-01-280-5500

Standard Form 298 (Rev. 2-89)
Prescribed by ANSI Std. 239-18
298-102

Approved for public release; distribution is unlimited.

BUBBLE INJECTION UNDER BREAKING WAVES

James B. Tannahill
Lieutenant, United States Navy
B.S., United States Naval Academy, 1990

Submitted in partial fulfillment
of the requirements for the degree of

MASTER OF SCIENCE IN METEOROLOGY AND PHYSICAL OCEANOGRAPHY

from the

NAVAL POSTGRADUATE SCHOOL
December 1996

ABSTRACT

Wave energy dissipation due to bubble penetration and inferred turbulent penetration from breaking waves in the surf zone is related to the total energy of dissipation. Bubble injection is inferred from void fraction measurements obtained using a 2.3 meter vertical array of eight conductivity sensors extending from the bottom through the water surface. Potential energy and dissipation associated with bubble injection are calculated and compared with total wave dissipation. Total wave dissipation is calculated from the energy flux balance measured using an array of seven pressure sensors in the surf zone.

Percent of total wave potential energy of the bubbles due to spilling breakers is on the order of 0.18% to 0.62%, consistent with past measurements in the surf zone. Percent of the bubble potential energy dissipation rates to total wave dissipation in the cross shore direction is on the order of 8% to 20%. The potential energy dissipation is largest immediately after injection, decaying exponentially after that. Bubble potential energy dissipation results within 1.2 seconds even for void fraction events greater than 36% and usually in less than 1.0 seconds. Energy dissipation was found linearly related (0.95 correlation coefficient) with the ratios of wave height to water depth, a measure of the percent of breaking waves within the surf zone.

TABLE OF CONTENTS

LIST OF FIGURES

LIST OF SYMBOLS

α	void fraction
β	beach slope
ε	dissipation
$\gamma(w)$	specific weight of water
η	surface elevation
π	constant equal to 3.1415
θ	angle of waves from normal to the beach
ρ	density of seawater
μ	conductivity
e	energy in joules
E	energy flux density
g	acceleration due to gravity

ACKNOWLEDGMENTS

I would like to thank Distinguished Professor Edward B. Thornton and Timothy P. Stanton, my primary advisors for their expertise and guidance to the very end. I would also like to thank the Project Manager, Robert Wyland, and the video team of Tom C. Lippmann and Chuck Worley, along with those who gave their time to make this project work from the ground up: James Stockell, Mary Bristow, Edie Gallagher, Ron Cowen, Andy Anderson, Jeff Helms, Bruce Morris, Carl Hager, Antonio Faria and Craig Norheim. Most of all my wife, Sheryl, and sons, Nicholas and Jacob, for allowing me the time to do all the necessary work. And finally, my parents, for their untiring devotion to all their children.

I. INTRODUCTION

Bubbles are entrained into the water column during wave breaking. Work is required to inject the bubbles into the water column resulting in the conversion of the potential and kinetic energy of the wave into potential energy associated with the buoyancy force of the bubbles. As the bubbles rise and enter the atmosphere at the surface, this potential energy is lost, and so acts as an effective mechanism for the energy dissipation of breaking waves. Bubble injection under breaking waves is important in the dissipation of wave energy, gas exchange at the air-ocean boundary, sound generation and sound speed alteration and the transport of organic material.

The objective of this paper is to demonstrate that bulk void fraction as a measure of bubble content can be accurately acquired in the surf zone utilizing vertical arrays of conductivity sensors and a knowledge of the water surface. Wave energy dissipation rates due to bubble injection under breaking waves can be calculated from these measurements. Dissipation rates due to bubble injection are compared with total wave dissipation calculated as the change in measured wave energy flux data acquired from a cross shore pressure array. Bubble injection dissipation is then correlated with wave height and percentage of breaking waves in the surf zone.

II. BACKGROUND AND METHODOLOGIES

A. BACKGROUND

Previous studies of bubbles injected by breaking waves are divided into discussion of breaking waves within the surf zone and breaking waves in deep water. Within the surf zone, Horikawa and Kuo (1966) postulated that the turbulence caused by bubble entrainment is the main source of energy dissipation after wave breaking, that the kinetic energy of turbulence decays exponentially in the vertical with time and is inversely proportional to the horizontal distance from the breaking point. Fuhrboter (1970) assumes bubble injection is the transfer mechanism from the energy of the wave to turbulent motion and finally frictional heat. He surmised (incorrectly) that the bubbles injected into the water column are advected along at the speed of the wave. Further assuming a uniform distribution of bubbles, he calculated wave energy would be dissipated within one wavelength for plunging breakers and multiple wavelengths for spilling breakers. Fuhrboter conceded that the distribution and concentration of air [under breakers] was virtually unknown, as there was no tank or in-situ data to support his claims. Since Fuhrboter, numerous attempts have been made to measure the distribution of bubbles injected by breaking waves, and to estimate the wave energy dissipated. Jansen (1986) used the term jet splashes to indicate bubble injection events in shallow spilling and plunging laboratory waves. He noted that several jet splashes occurred for both plunging

and spilling breakers after the initial breaking, indicating that several of these bubble injection events were necessary to dissipate the energy of the wave. Hwung, Chyan and Chung (1992) confirmed Kuo and Horikawa's postulation that the concentration profiles of air bubbles decay exponentially in the horizontal direction and added that they decay hyperbolically in the vertical direction. Their energy balance shows that the loss of the wave potential and kinetic energies between the impinging point of the breaking wave into the water surface and the maximum bubble injection depth is nearly balanced by the increase of potential energy of the air bubbles, implying that bubble injection is the dominant wave dissipation mechanism.

Deep water wave tank and field experiments have revealed the importance of bubble injection in the open ocean. Medwin and Brietz (1989) hypothesized and demonstrated a bubble generation layer immediately below the free surface with an underlying dispersion layer that is dominated by buoyancy and turbulent effects. Lamarre and Melville (1991,1992) postulated that the dissipation due to air entrainment should be correlated with the energy of breaking waves. They found that the work required to keep air entrained against the buoyancy force per unit width also correlated with the energy of breaking waves. They surmised that downward advection of fluid should balance the upward motion of the bubbles. Gemmrich (1992) showed that the bubbles are injected to a depth dependent on the buoyancy of the bubble and turbulent forces of open ocean breaking waves. He determined that void fraction

distribution is a function of depth and penetration depth is a function of the wave height and type of breaker. Loewen and O'Dor (1996) calculated the energy required to submerge a single bubble to a certain depth as a function of the volume of the bubble and the specific weight of seawater. They postulated that by knowing the size distribution of bubbles in a certain depth of penetration, the energy dissipated by bubble injection could be accurately calculated.

B. METHODOLOGIES

The extent of penetration and size distribution of the penetration events have been studied by various methods. Breaking waves have been simulated in both fresh and salt water tank experiments and the bubble injection has been measured using UV light and styrene balls, lasers, impedance and conductivity probes, video and still photography and/or sound. These methods work well in the laboratory, but in-situ measurements of bubble injection have been harder to obtain due to the difficulty of placing instruments in ocean waves and maintaining them and the infrequency of substantial injection events in the open ocean.

LaMarre and Melville (1991,1992), using a conductivity probe, found the fraction of deep water breaking waves was dependent on the significant wave height and wind speed. Lamarre and Melville (1994) found that 30% to 50% of the energy due to breaking of plunging breakers is dissipated via bubble injection, while only 0.4% to 3.0% of the total energy due to spilling breakers is dissipated in this manner. They addressed the problem of comparing 2-D data

with 3-D data showing that 3-D data allows for lateral spreading of the wave and determines which part of the wave (the center or side edge) crosses the detecting array. Haines and Johnson (1995) and Loewen and O'Dor (1996) utilized photographic techniques to analyze the size distribution of injected bubbles in spilling breakers in fresh and salt water, noting little distribution difference between the two mediums beneath large waves. Their findings, however, confirmed previously known differences in bubble characteristics with salt water having more, smaller bubbles while occupying essentially the same air volume as freshwater and longer residence times for bubbles in salt water due to buoyancy and friction effects. Since many tank experiments have been done in tanks with only fresh water, the difference in bubble size distribution with salt water could have marked effects on the injection patterns, distributions and amount of energy dissipated. Showing only a small amount of energy dissipation due to bubbles (0.05% to 0.4%) in spilling breakers, Loewen and O'Dor (1994) also indirectly showed that differences in data collection and data analyses methods greatly effect experimental results. Jansen (1986) coupled a UV light with near neutrally buoyant fluorescent particles to track regions of high aeration in a wave tank. His plunging breakers on a gently sloping beach (1:30) showed several jet splash motions from each breaking wave, each splash causing bubble injection and further complicating the relationship between the breaking wave height, bubble injection extent and dissipation calculation. He noted that the first two jet splash motions accounted for only 5% each of total energy dissipation,

but that later injection events accounted for up to 20% dissipation each. Su and Cartmill (1993) utilized four resistive gauges in a vertical array on a tethered float to compute void fraction. He characterized the probabilities of certain void fractions of up to 40% for certain wind speeds in the open ocean. He analyzed SWADE wave data to obtain wave breaking events at 0.25 m below the surface of the open ocean. He also used an acoustic resonator originally designed by H. Medwin of the Naval Postgraduate School (NPS) to measure in-situ size spectra of bubbles in the 30 to1200 micron range for bubble injection effects on low frequency sound speed near the surface. Asher and Farley (1995) utilized a phase-doppler laser anemometer to simultaneously measure the size and velocity of a bubble, although particle concentration measurements were questionable due to problems with unquantified particle and flow trajectory effects. Gemmrich (1992) utilized four conductivity cells in a 1.14 m vertical array suspended from a floating platform to determine frequency of bubble injection events, penetration depth of such events and event duration in open ocean. He found that the average void fraction event of 10% lasted only on the order of 0.5 s and even void fraction events greater than 40% lasted no more than 1.3 s.

In the following sections, a description of a portion of the Monterey Bay Beach Experiment (MBBE 1996), methodology of data analysis, results and conclusions are presented. Results show the detection and representation of

bubble injection events, percentage of total energy dissipated and percentage of energy dissipation rate due to bubble injection.

III. EXPERIMENT AND DATA ANALYSIS

A. INSTRUMENTATION AND CALIBRATION

An experiment was conducted 3 to10 May 1996 at Del Monte Beach in Monterey, California, to measure wave transformation and the distribution of void fraction over the vertical within the surf zone. A 4.6 m steel pole was jetted vertically extending 2.3 m above the bottom. Eight FSI inductive conductivity sensors were mounted on the pole with variable spacing of 0.19 to 0.37 m. The measurement cavities of the conductivity cells were aligned at 45° to the vertical with a digital level accurate to 0.1°. The 45° upward tilt towards the sea represents a compromise accommodating the primarily horizontal velocity of shallow water waves and allowing bubbles to escape upward without being trapped in the 0.0165 m diameter cylindrical measurement cavity (Figure 1). A thermistor, designed and built at NPS, accurate to 0.002° C, a Hydracon strain gage pressure sensor and a vertical array of eight electromagnetic conductivity meters were also attached to the pole (Figures 2 and 3). A cross-shore horizontal array of seven Hydracon pressure sensors affixed to a chain and spaced 17 m apart spanned 102 m of the surf zone and lay on the bottom directly adjacent to the vertical array. The vertical array was located between sensor numbers 4 and 5 (Figure 4). The beach and all equipment were surveyed daily with a laser ranging system accurate to within 0.04 m.

SENSOR OUTLINE DRAWINGS

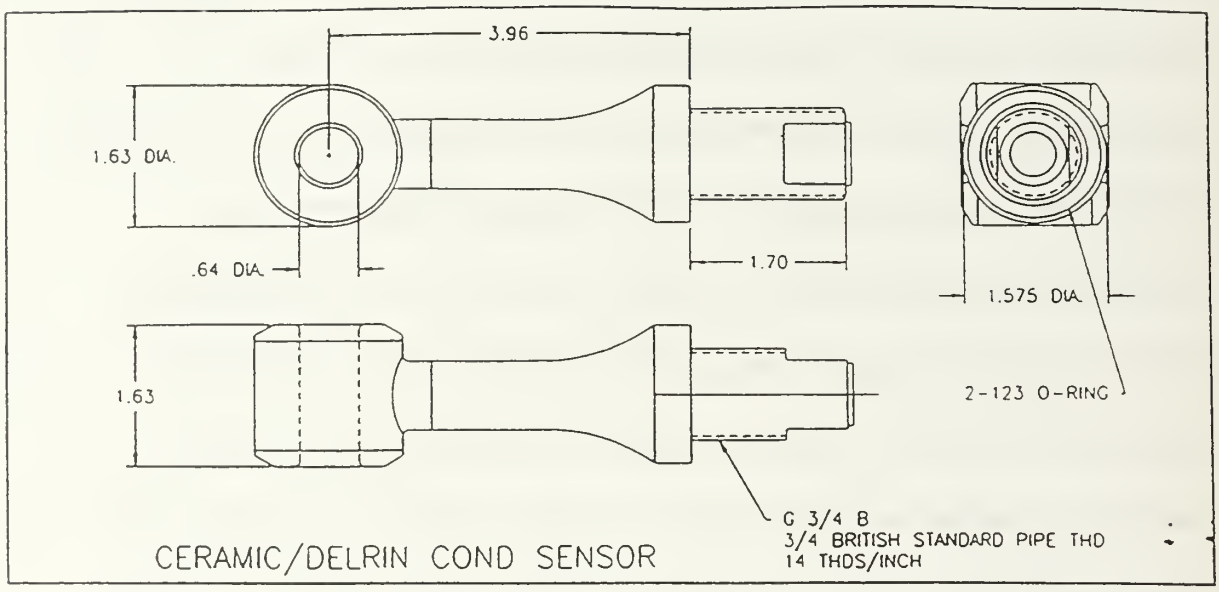

STANDARD C-T SENSOR

Figure 1. FSI Conductivity Sensor

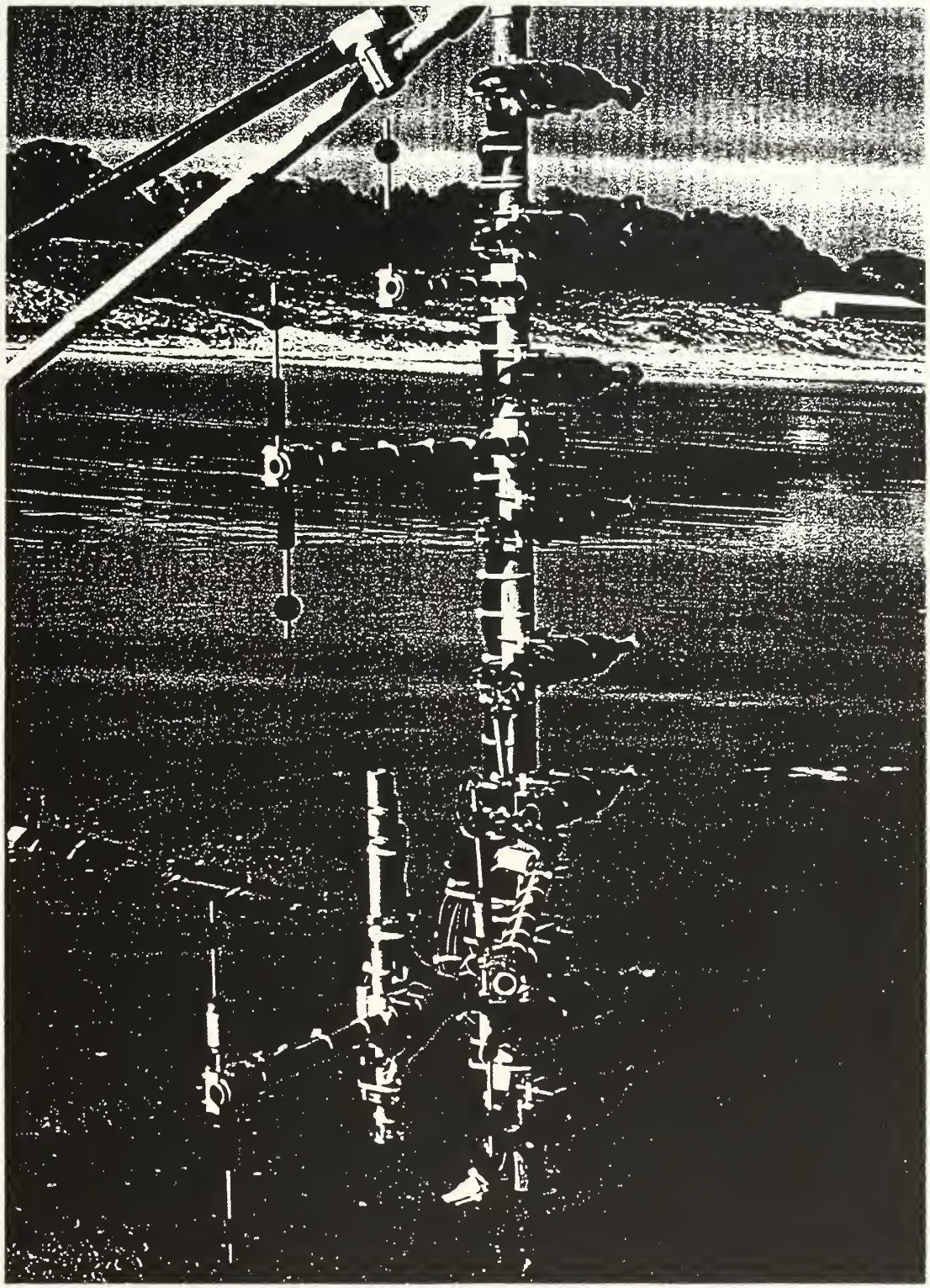

Figure 2. Photo of the Vertical Array Installed at Del Monte Beach, May 96

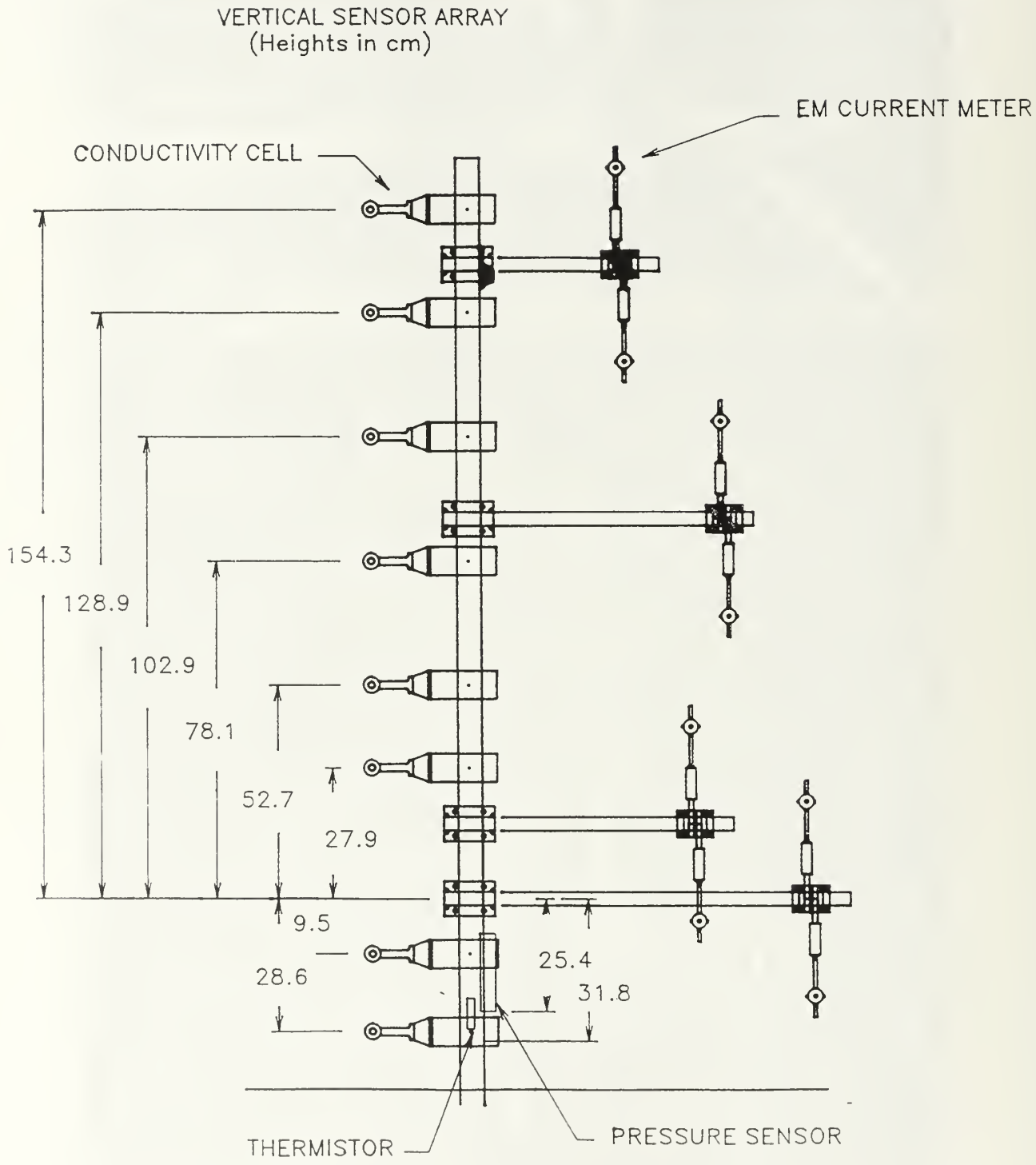

Figure 3. Schematic of the Vertical Array Sensor Diagram, showing location of conductivity cells, pressure sensor and thermistor with electromagnetic current meters also shown.

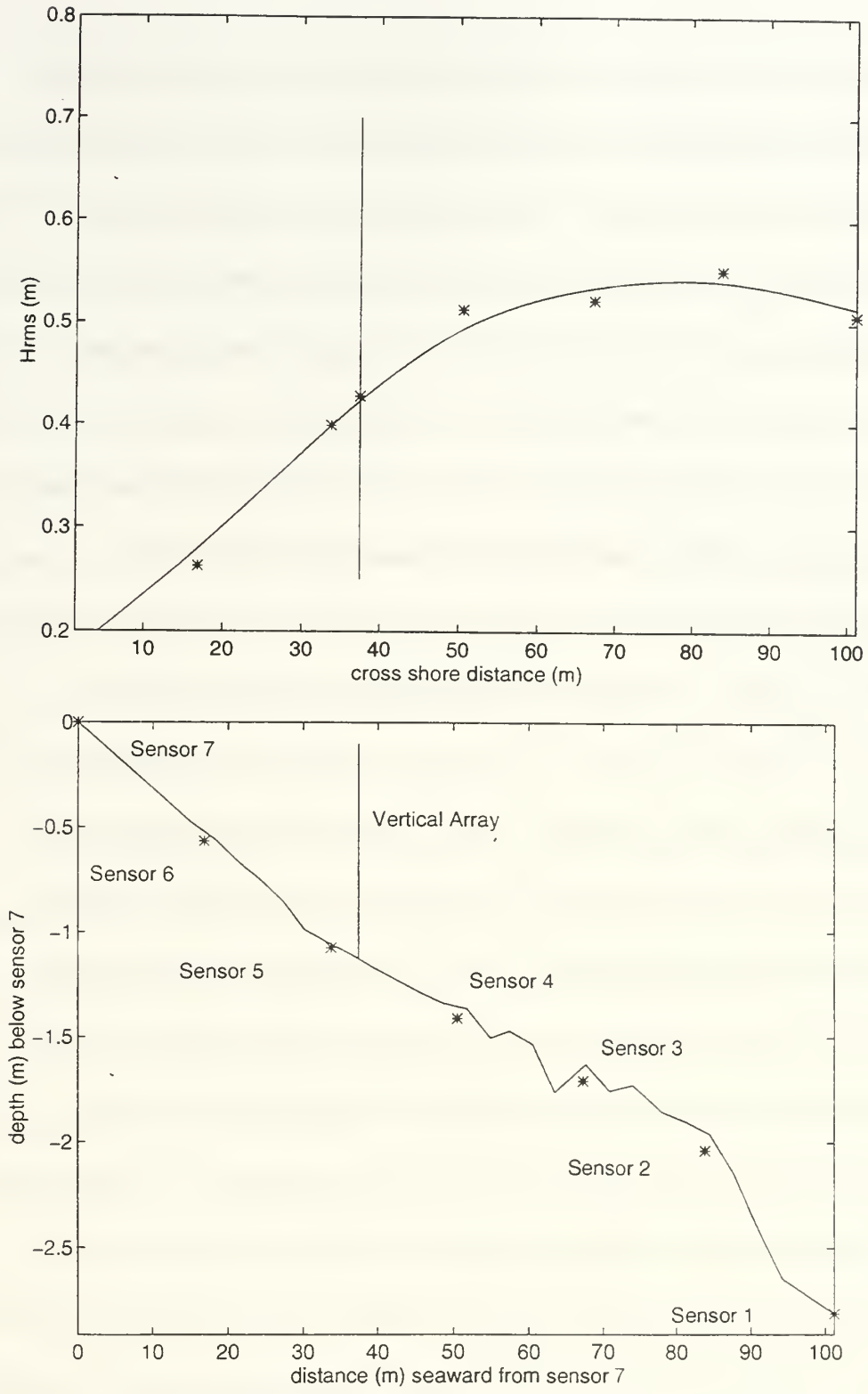

Figure 4. Cross-Shore Pressure Sensor Array Bathymetry, showing location of vertical array (lower) and H_{rms} wave height (upper) for the seven pressure sensors and the vertical array

The wave field during the measurements consisted of 0.30 m to1.0 m breakers with mostly spilling, some plunging, on a beach with a slope of 1:36 in the proximity of the vertical array. Small ripples approximately 0.50 m in wavelength and 0.01 m to 0.04 m in amplitude were frequently observed in the beach morphology in the vicinity of the vertical array. Waves approached essentially normal to the nearly straight and parallel bottom contours. Instruments were installed at low tide and data acquired over high tides during the six day period. Tides in the Monterey Bay are semi-diurnal. Water temperatures ranged between 14 and 16 degrees Celsius. The water column during data acquisition was believed to be well mixed with no significant temperature or salinity gradients. No significant weather occurred locally. Atmospheric pressure was measured using a Paroscientific digital barometer accurate to 0.01mb, approximately 70 m inland of the vertical array. Water pressure, temperature and conductivity data were sampled at 48 Hz on the vertical array, while the cross shore array pressures were measured at 8 Hz.

Video data were recorded around the clock with both day and night cameras that referenced several fixed data points on the beach. The data were obtained from two angles: directly shoreward from the vertical array by night camera and approximately 100 m south of the array by day. The video was used to establish breaker type and note the position of the breaker line relative to the vertical array.

Hydracon pressure sensor, thermistor and conductivity cell calibrations were performed at the NPS Oceanography Calibration Laboratory. The pressure sensors were subjected to a water bath of temperatures ranging from 10° to 20° C by 2.5° C increments at four (cross shore array) or five (vertical array) different water head levels ranging from 0.0 m to 2.0 m. The conductivity cells were immersed in five baths of different salinities at constant temperature and a fixed salinity water bath at temperatures ranging from 10° to 20° C by 2.5° C increments. The salinities were measured using an Autosal precision salinity device accurate to 0.0001 ppm. The thermistors were calibrated 0.002° C. The barometer was calibrated by Paroscientific, Inc. in Redmond, Washington.

B. ANALYSIS

Data collected over 1.4 days from 8 to 10 May 1996 at Del Monte Beach in Monterey Bay, California are analyzed. Conductivity variations due to vertical mean temperature and salinity are eliminated by normalizing the top seven sensors with the bottom sensor after applying a mean offset for the maximum value of each conductivity sensor compared with the maximum value of the bottom sensor over 20 minute time series at 0.1 second averages. It is assumed that the bottom sensor was totally immersed in seawater for the examined data set and did not experience any bubble injection events, thereby acting as a maximum value for conductivity at each time step. A condition that a minimum of two sensors at the bottom be covered with water during periods of analysis was

used to ensure few, if any void fraction events are contaminating the maximum value of the bottom sensor.

Void fraction is determined from the measured conductivity using a simplified Maxwell's expression for effective conductivity ($\mu_{effective}$) of a medium where noninteracting spheres of a certain conductivity (air) are immersed in a medium of a much higher conductivity (saltwater):

$$\mu_{effective} = ((1 - \alpha)/(1 + \alpha/2))\ \mu_{seawater}, \quad (1)$$

where $\mu_{seawater}$ is the conductivity of seawater and α the volumetric fraction occupied by the air (void fraction) (Maxwell, 1891). Solving for void fraction,

$$\alpha = \frac{2\,(1 - \mu_{effective}/\mu_{seawater})}{(1 + \mu_{effective}/\mu_{seawater})}, \quad (2)$$

where $\mu_{effective}$ is the measured conductivity of the top sensors which are within the water, and $\mu_{seawater}$ is the conductivity of the bottom sensor. Conductivity data acquired at 48 Hz was averaged to 0.1 second time steps commensurate with the temporal response of the conductivity cells.

Water surface elevation, η, is calculated using data from the pressure sensor attached to the vertical array and compared to the interpolated value from the seven sensors in the cross shore array. The pressure signal is converted to a surface elevation time series by first calculating the complex Fourier spectrum of 20 minute time series, applying the linear wave theory transfer function and then inverse transforming the record.

The upper sensors were in and out of the water as the waves passed the vertical array. An example of a 20 second time series of the conductivity measurements for three upper sensors along with the water surface, η, is shown in Figure 5. Cell 4 is positioned at elevation 1.03 m about 0.25 m above the mean water level and shows indications of being hit by waves only during the peaks of the water surface. When the sensor is out of the water the value goes to zero. Cell 5 is at an elevation of 0.98 m and drops in conductivity values for Cell 5 correlate with the decrease in surface elevation. Cell 6 shows less severe indications of bubble injection events, as its elevation is 0.25 m below mean water level ensures that it is immersed during this time series. Several bubble injection events penetrate to the depth of Cell 6, most notably at 12 and 17 seconds during the time series.

The fixed heights of the conductivity sensors are referenced to η and when the sensors were within 0.05 m beneath the surface for a time step, they were removed from the data set. A depth of 0.05 m below the surface was chosen as a conservative estimate to eliminate very low conductivities entering averages due to errors in the η estimate when a sensor was actually out of the water. For example in Figure 5, the readings at Cell 4 are essentially discarded, since the first 0.05 m below the water surface has been eliminated. Any void fraction event that may have occurred in the lag time is eliminated because the level of the sensor is considered below the water surface. Also, some of the bubbles at the immediate surface of the water due to the advection of the bore

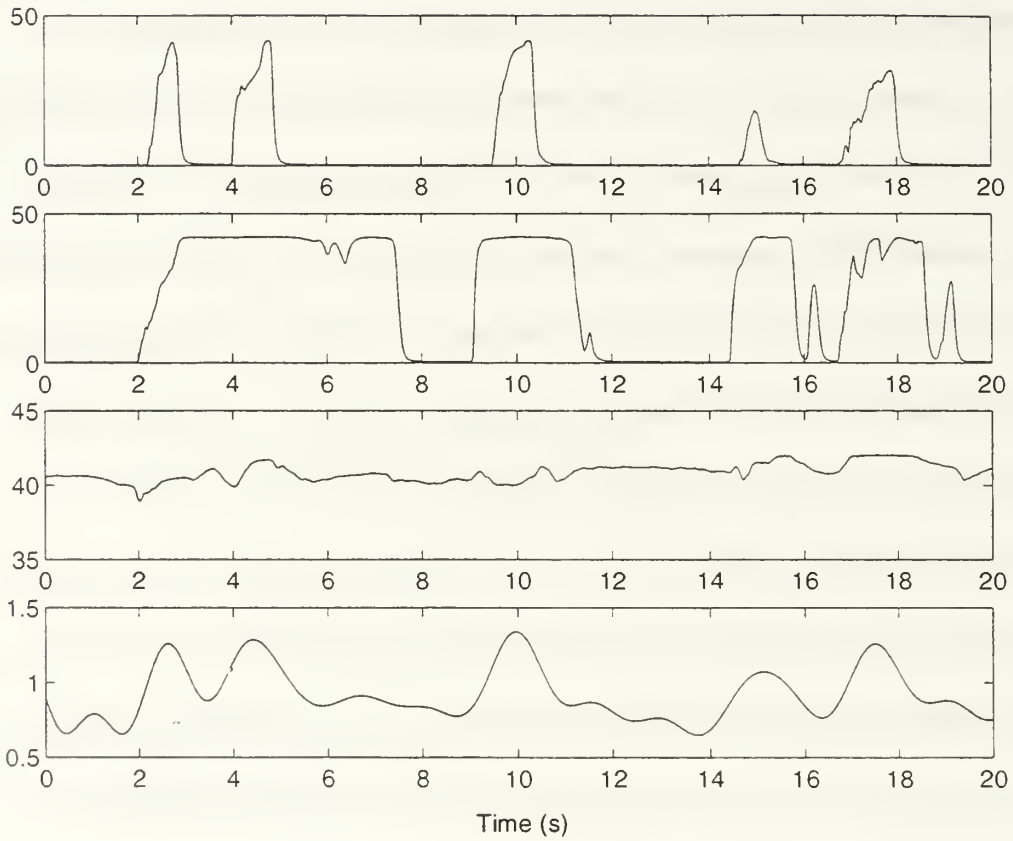

Figure 5. Conductivity of Cells 4, 5 and 6 and Water Surface vs. Time

are eliminated from true bubble injection by excluding the top 0.05 m. Conductivity data were converted to void fraction using Equation 2 and inserted into dz = 0.05 m bins beneath η for each 0.1 second time step.

The potential energy per unit area of the air entrained due to bubble injection at the 0.1 second time steps is calculated (see for example LaMarre and Melville, 1992):

$$E_b(t) = \frac{\rho g}{T} \int_{-h}^{\eta} \propto(z,t)\, z\, dz\,, \tag{3}$$

where values of buoyancy force, $\rho g \alpha(z, t)$, are multiplied by the depth below the surface, z, of the center of the bin, dz.

Production of potential energy by bubble injection and subsequent dissipation is calculated by differentiating $E_b(t)$ with respect to time:

$$\varepsilon_b(t) = \frac{dE_b}{dt}\,, \tag{4}$$

Therefore dissipation is the time average of the negative values of Equation 4. The time averaged bubble injection dissipation, $\langle \varepsilon_b \rangle$, is compared with the total wave dissipation $\langle \varepsilon \rangle$, which is calculated from the energy balance equation. Assuming the wave field is stationary and the bottom contours are straight and parallel:

$$\frac{\partial EC_{gx}}{\partial x} = \langle \varepsilon \rangle, \tag{5}$$

where E is the total wave energy, C_{gx} is the group velocity of the waves in the onshore direction, x. The C_{gx} is calculated from linear theory using the peak frequency of the wave spectrum and the measured depth.

Total wave energy (E) is calculated using the linear wave theory relationship:

$$E = 1/8\ \rho g\ H_{rms}^2, \tag{6}$$

which assumes the wave heights are Rayleigh distributed. The η time series is obtained from the pressure data from the cross shore array. H_{rms} is calculated:

$$H_{rms} = \sqrt{8}\ (\sigma_\eta), \tag{7}$$

where σ_η is the standard deviation of the band passed (0.05-1.0 Hz) surface elevation time series calculated from the pressure data.

An example of the energy spectrum of the surface elevation at the vertical array (Figure 6) shows a relatively broad spectrum with a peak at 0.18 Hz indicative of locally wind generated waves. A lower frequency component at 0.008 Hz due to the wave groups observed approximately every two minutes and has been removed by high pass filtering. This spectrum is taken from the afternoon, when the sea breeze is the strongest and wind generated waves in the Monterey Bay are at their maximum heights.

Mean water levels at the vertical array averaged over 20 minutes, were calculated utilizing the mean pressure data after subtracting the barometric pressure. The tidal variation was small during the six hours of analyzed data (1430-2030 PST), with an initial rise of 0.10 m then a fall of nearly 0.30 m

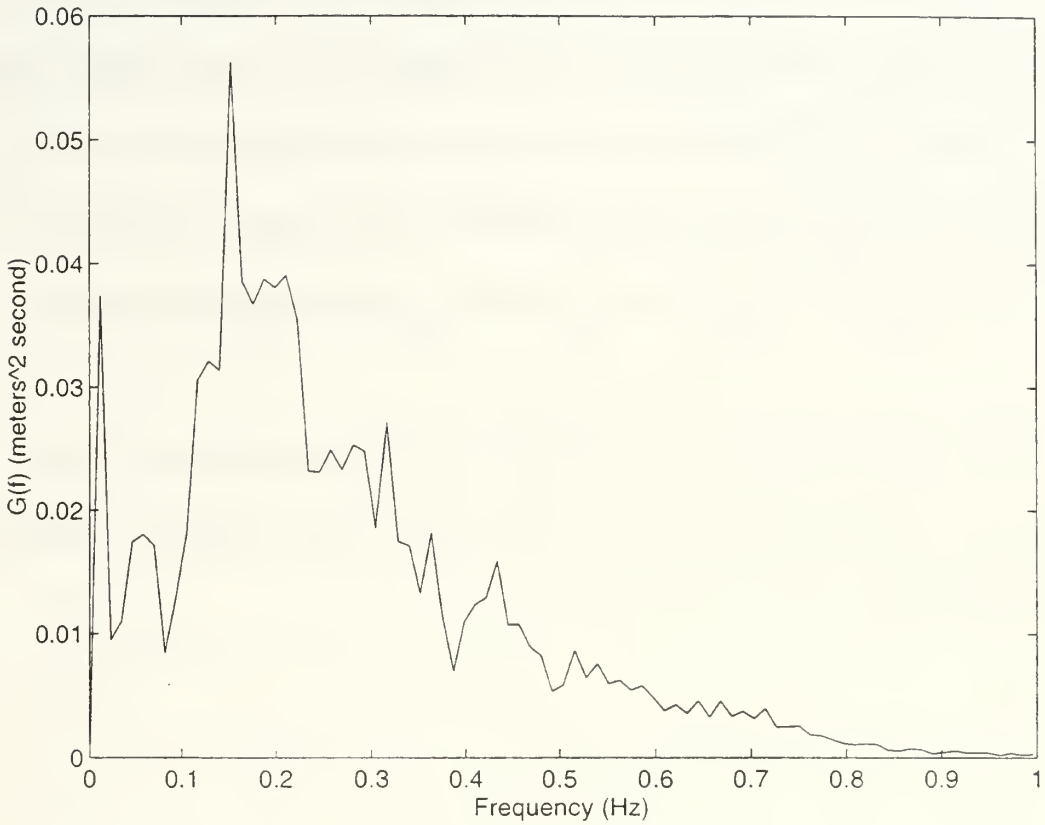

Figure 6. Energy Spectrum of Water Surface Elevation vs. Frequency

(Figure 7, upper panel). The tide is the lower of the high tides for the day attributed to the diurnal portion of the mainly semi-diurnal tides. The measured values were utilized in the calculation (η), and subsequently for referencing the depth of void fraction to the water depth.

The H_{rms} wave heights averaged over twenty minutes (Figure 7, lower panel) show small variation starting at 0.32 m rising to 0.43 m then falling back to 0.33 m in response to the change in mean water level of the tide. The sea breeze was at its maximum in the late afternoon, adding energy in the form of wind generated, higher frequency waves, which correlates well with the rise in H_{rms}.

Video data were analyzed to determine if bubble injection events were caused by spilling or plunging breakers and location of the breaker line relative to the vertical array.

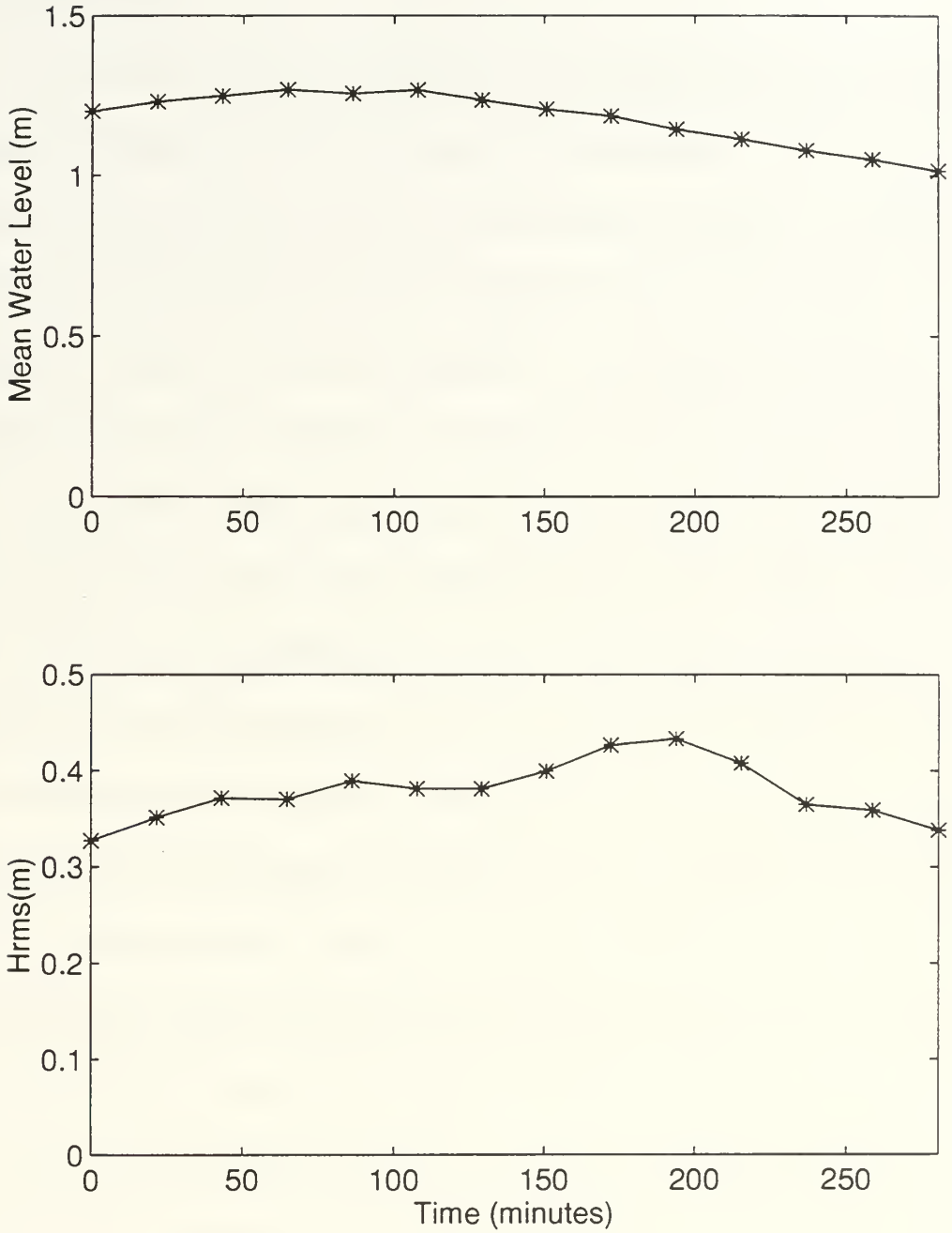

Figure 7. Mean Water Level (upper) and H_{rms} (lower) vs. Time at the vertical array

IV. RESULTS AND CONCLUSIONS

A. RESULTS

As the mean water level varied due to the tide, the relative location of the vertical array within the surf zone changed. An example of the cross-shore variation of H_{rms} at time 200 minutes (relative to time in Figure 7) shows the vertical array to be within the surf zone (Figure 4, upper panel). Maximum H_{rms} indicate the location of the mean breaker line. The mean breaker line was initially landward of the vertical array and moved seaward across the array at approximately time 180 minutes in Figures 7. The position of the breaker line just seaward of the vertical array correlates with the highest bubble injection dissipation rates and bubble injection energy. Unfortunately, the maximum H_{rms} values occur after the period when the breaker line was immediately seaward of the vertical array which would have provided more intense void fraction events. Energy due to bubble injection and energy production/dissipation rates along with η vs. time are shown in Figure 8. The peak values are attained near instantaneously from the bubbles being injected into the water column and the return to zero due to bubbles returning to the surface is nearly as quick--within one second in most all cases--less than 25% of the mean period of the waves. In certain cases, dissipation takes longer, but the surface elevation shows these cases to actually be two waves passing the vertical array within one second of each other. These results qualitatively agree with Gemmrich who observed

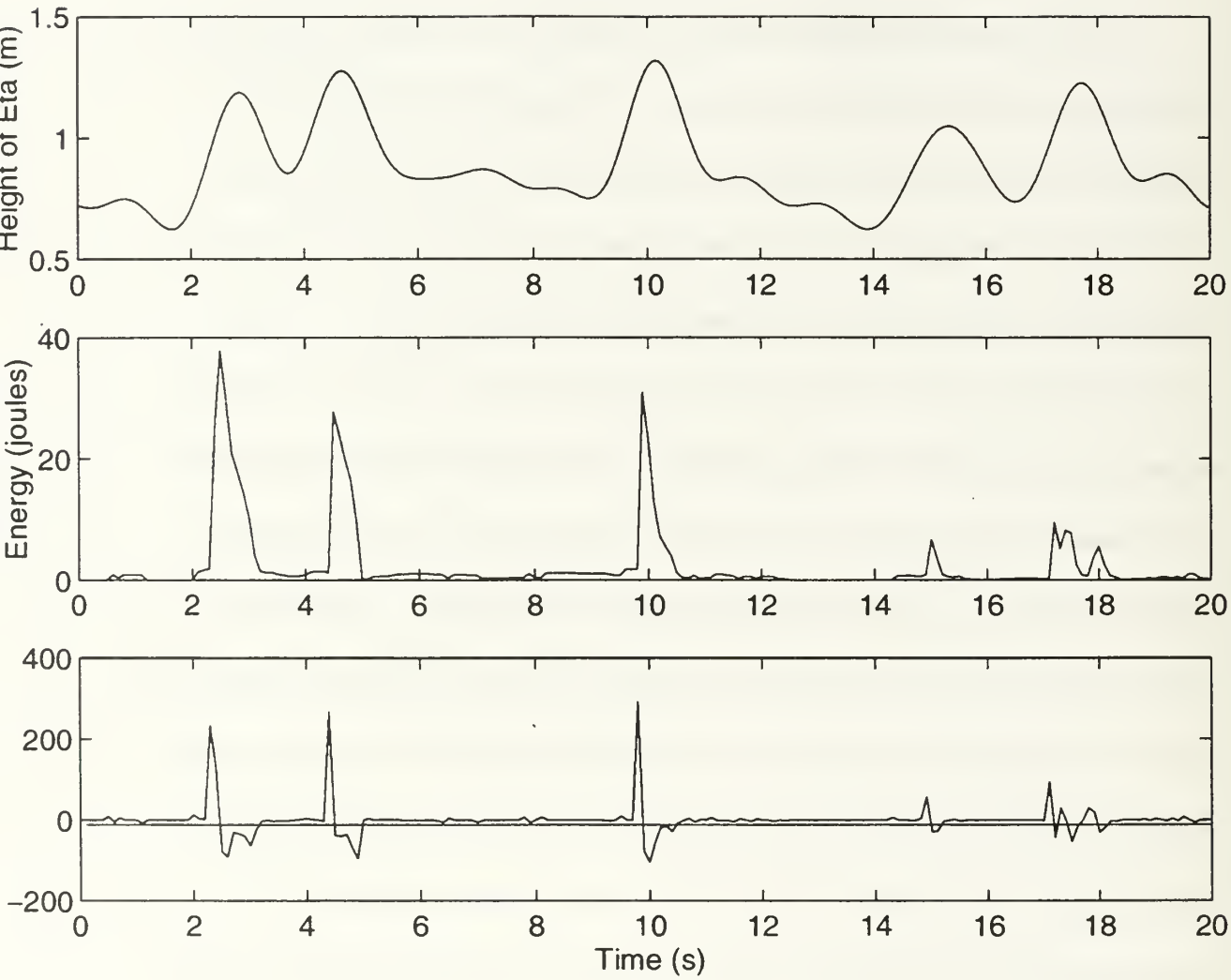

Figure 8. Water Surface Elevation (upper), Bubble Potential Energy (center), and Rate of Bubble Potential Energy Change (lower) vs. Time at the vertical array

decay time of energy dissipation of between 0.5-1.35 s for void fractions of up to 40%.

Void fraction is also calculated using Equation 2 from the conductivity measurements over the same 20 s time period in Figure 5 at the same time step of 0.1 s (Figure 9). Individual void fraction events can clearly be seen beneath the water surface. Few void fraction events penetrated below 0.50 m, with the majority of the bubbles being injected in the first 0.25 m. Void fractions as high as 36% were observed. Although these fractions seem high for spilling breakers, the duration of the injection events must be noted. Examination of the data found that even the most intense bubble injection events had residence times of no more than 1.2 s -- or less than 25% of the observed mean period wave of 5.3 seconds. Such short duration of intense bubble injection events reduces to a very small amount of energy in the mean.

Maximum E_b values are less than 40 joules and coincide with peaks in the water surface, η. Since the time of dissipation is usually less than 1 second, Bubble Potential Energy is dissipated at a rate of over 200 joules per second for individual 0.30-0.50 m bubble injection events.

Mean bubble potential energy due to bubble injection is small, on the order of 0.3-1.4 joules and peaks when the breaker line is ahead of the vertical array between minutes 180-220 (Figure 10, upper panel). The total wave energy, E, is calculated from the cross shore array H_{rms} and varied between 130-290 joules (Figure 10, center panel). The ratio of the mean bubble potential

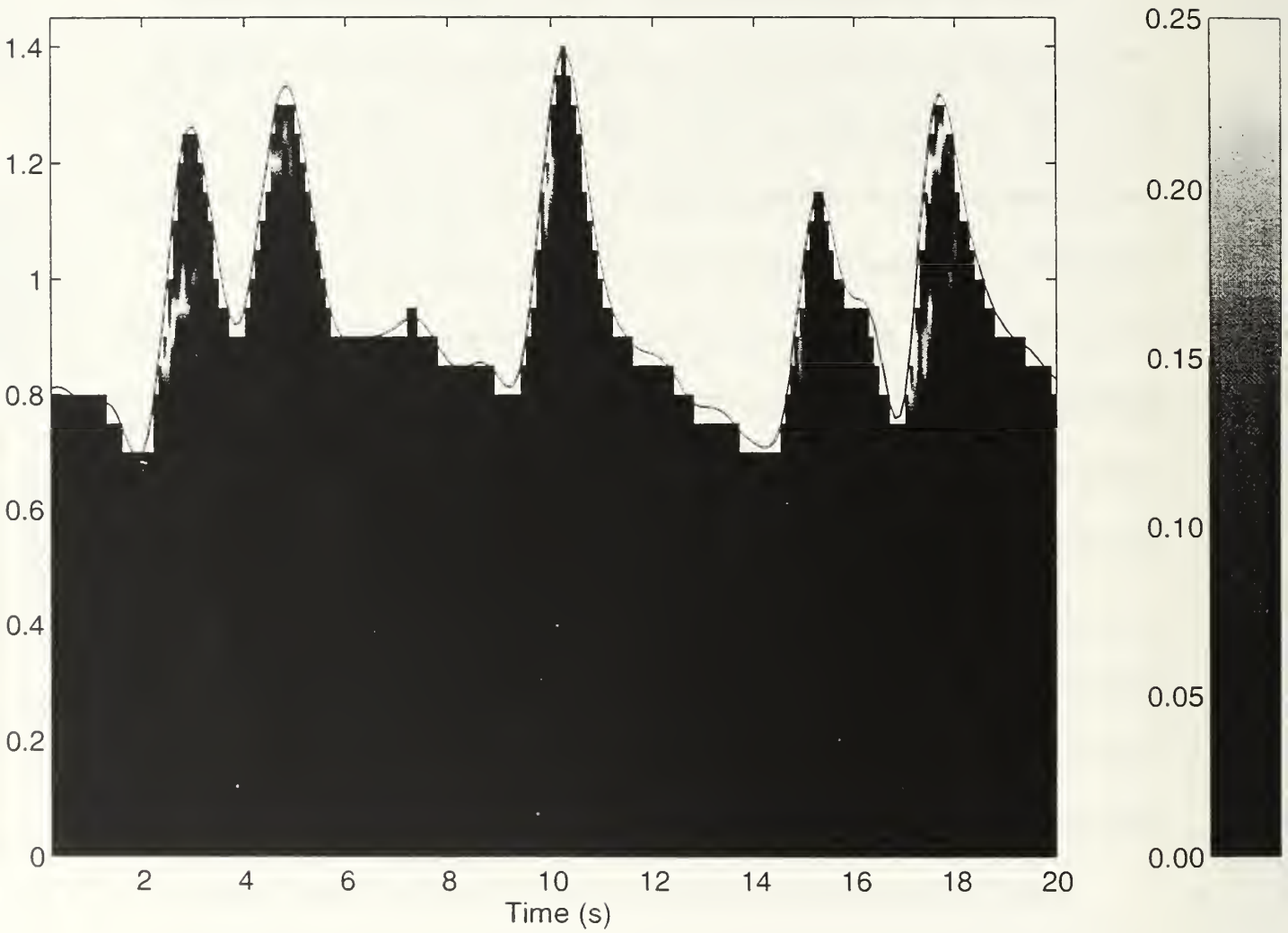

Figure 9. Void Fraction Penetration Below the Water Surface (η) vs. Time

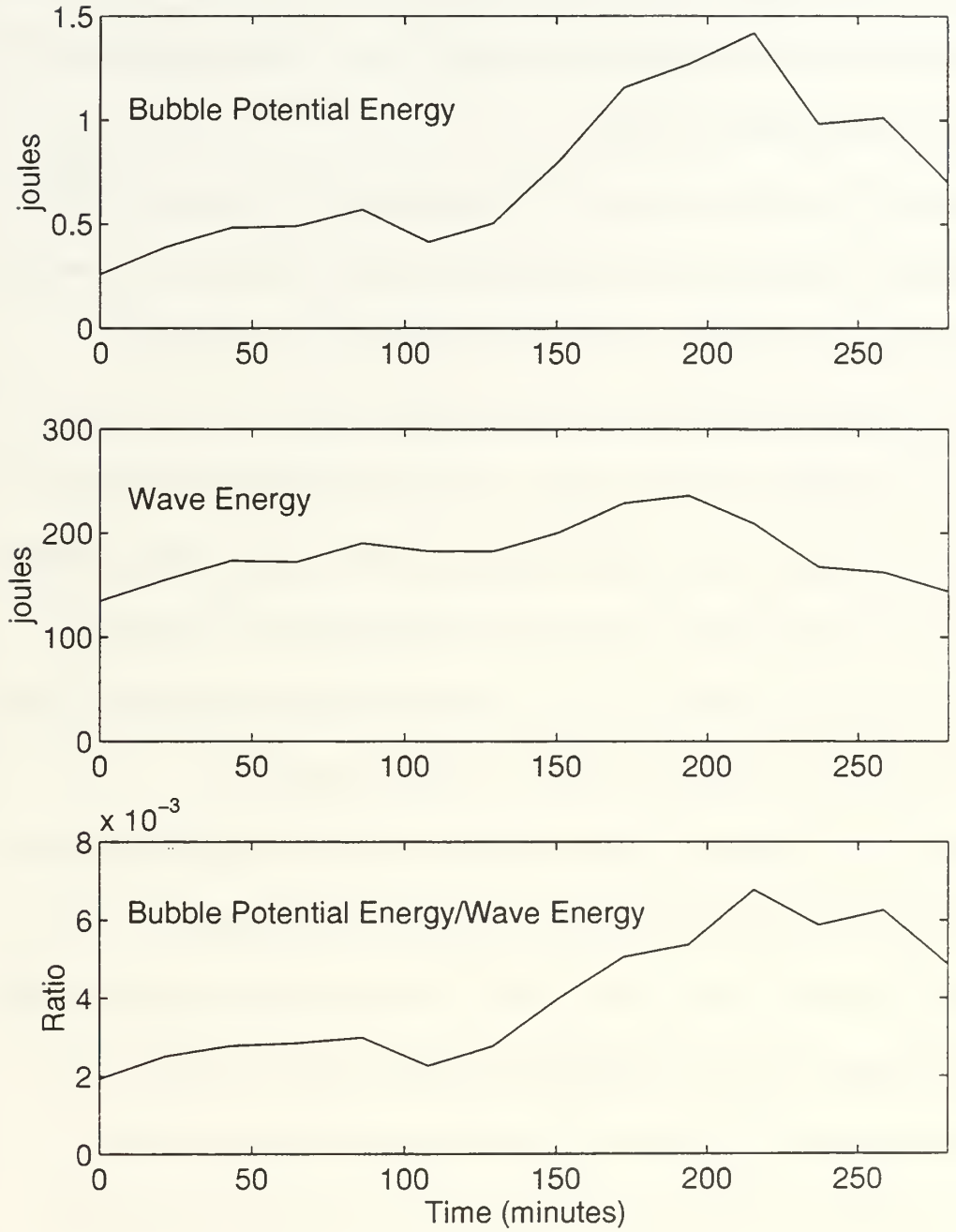

Figure 10. Bubble Potential Energy (upper), Total Wave Energy (center), and their Ratio (bottom) vs. Time at the vertical array

energy to total wave energy is on the order of 0.02-0.7% and peaks where the breaker line is just seaward of the vertical array (Figure 10, lower panel). These results are in good agreement with Loewen and O'Dor's (1994) observations of 0.05-0.4% of total energy dissipated.

Twenty minute time averages of bubble dissipation ranged up to 8 Watts. The dissipation is largest when the breaker line is slightly seaward of the vertical array. Total energy dissipation, calculated as the change in energy flux (Equation 5) between cross shore pressure sensors number 4 and 5 over a 17 m distance is on the order of 20-50 joules/s. The maximum change in energy flux was when the breaker line was between the two sensors. The maximum bubble dissipation coincides with the maximum total wave dissipation. The energy dissipated by bubble injection rises more quickly than the total energy flux, going from 8 to 20% of the calculated energy flux, $\partial ECg/\partial x$ (Figure 11).

The top seven sensors on the conductivity array were normalized by the bottom sensor to account for the effects of changing bulk salinity and temperature over time. It was assumed that no bubble injection events reached the bottom sensor, that is that it remained at its peak value throughout acceptable data runs. If bubble injection events were reaching the bottom sensor, the conductivity measured by the other seven sensors would indicate lower void fractions than actually occurred. The analyzed data was chosen in close proximity to high tide to minimize errors due to the bottom conductivity bubble injection contamination. The water column is assumed well mixed in

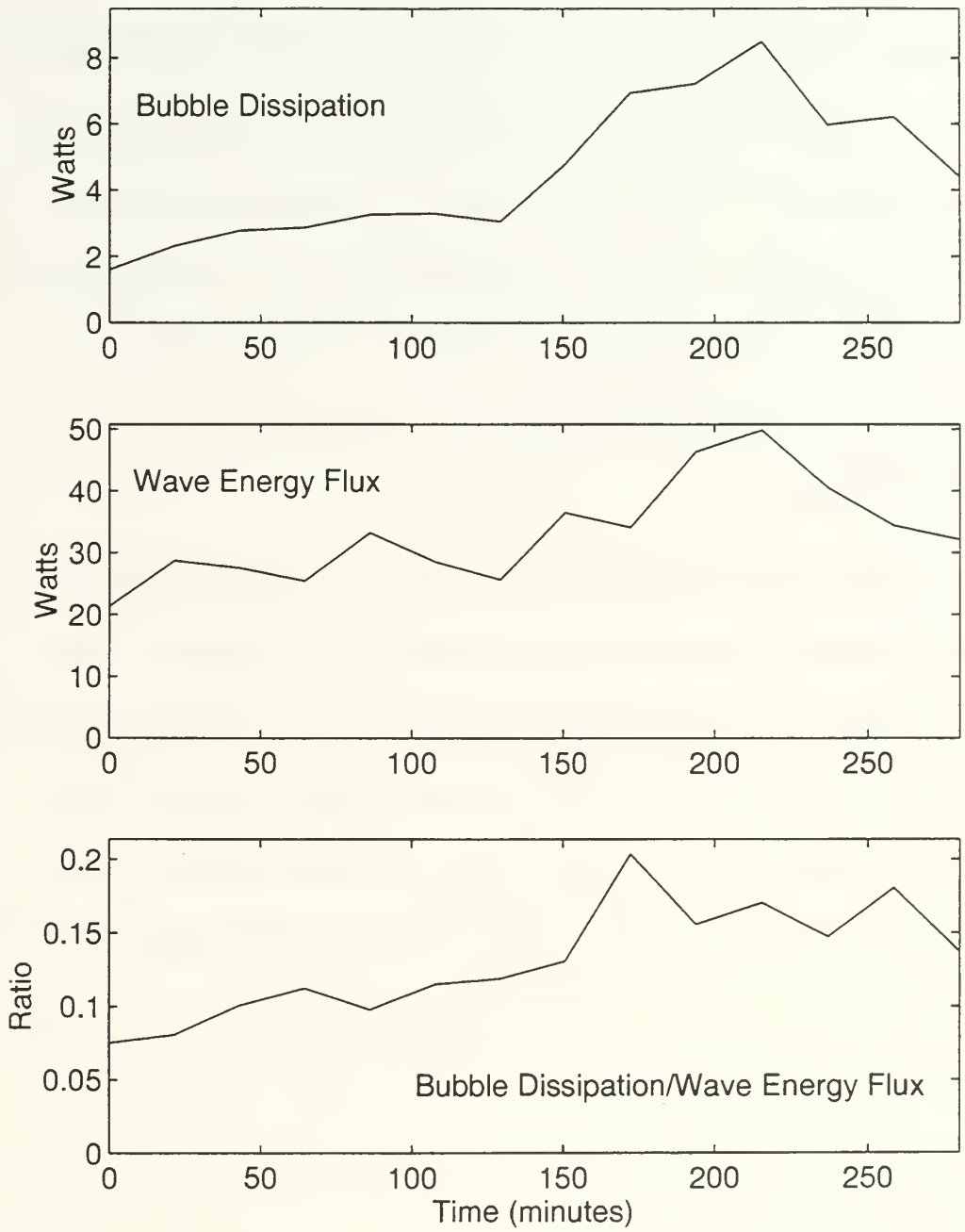

Figure 11. Bubble Dissipation (upper), Wave Energy Flux (center), and their Ratio (bottom) vs. Time across the vertical array

temperature and salinity at all periods of data acquisition due to the turbulent nature of the surf zone.

A measure of the fraction of waves breaking within the surf zone is given by $\gamma = H_{rms} / h$. Values of $\gamma = 0.4$ measured in the field are indicative that most waves are breaking with smaller values indicating a lower percent of breaking waves (Thornton and Guza, 1983). Bubble dissipation is found correlated with values of both H_{rms} and γ with a correlation coefficient of 0.65 and 0.96 respectively, which is statistically significant (Figures 12 and 13).

B. CONCLUSIONS

Void fraction injection depths of greater than 0.50 m were observed, but the majority of injection events were less than 0.40 m. H_{rms} during the largest void fraction events was on the order of 0.40-0.45 m and only when the breaker line was at or just seaward of the vertical array were injection depths greater than 0.40 cm. Although individual bubble injection events showed up to 36% void fraction, overall void fraction percentages in fourteen 20 minute time series show a mean of less than 4% (Figure 14). Void fraction maximums were seen at wave group intervals of approximately two in the 20 minute time series and individual bubble injection events were clearly visible in the 20 s time series with injection depths to over 0.45 m.

Percent of total wave potential energy of the bubbles due to the spilling breakers is on the order of 0.18-0.62%. This is consistent with past

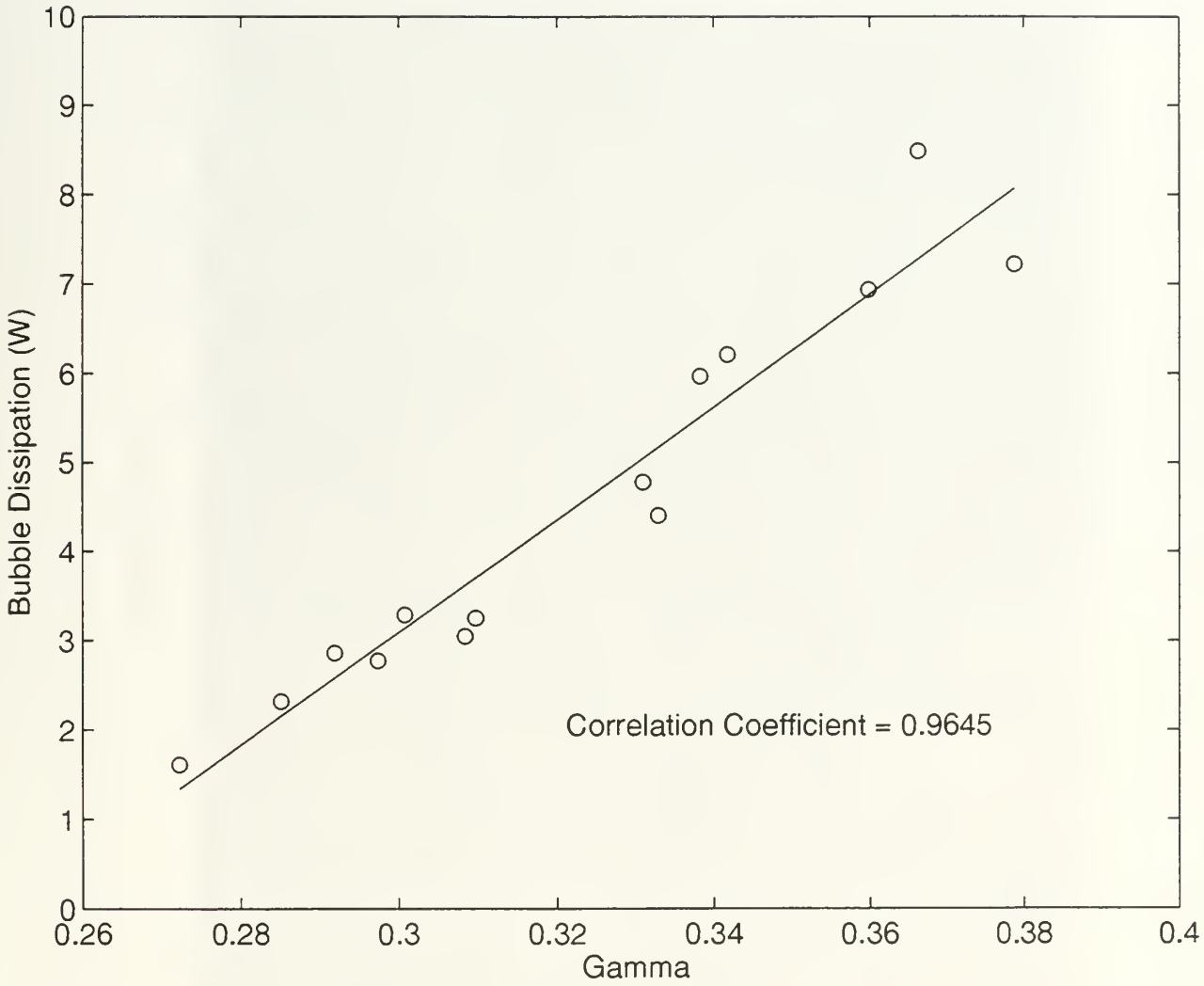

Figure 12. Bubble Dissipation vs. Gamma

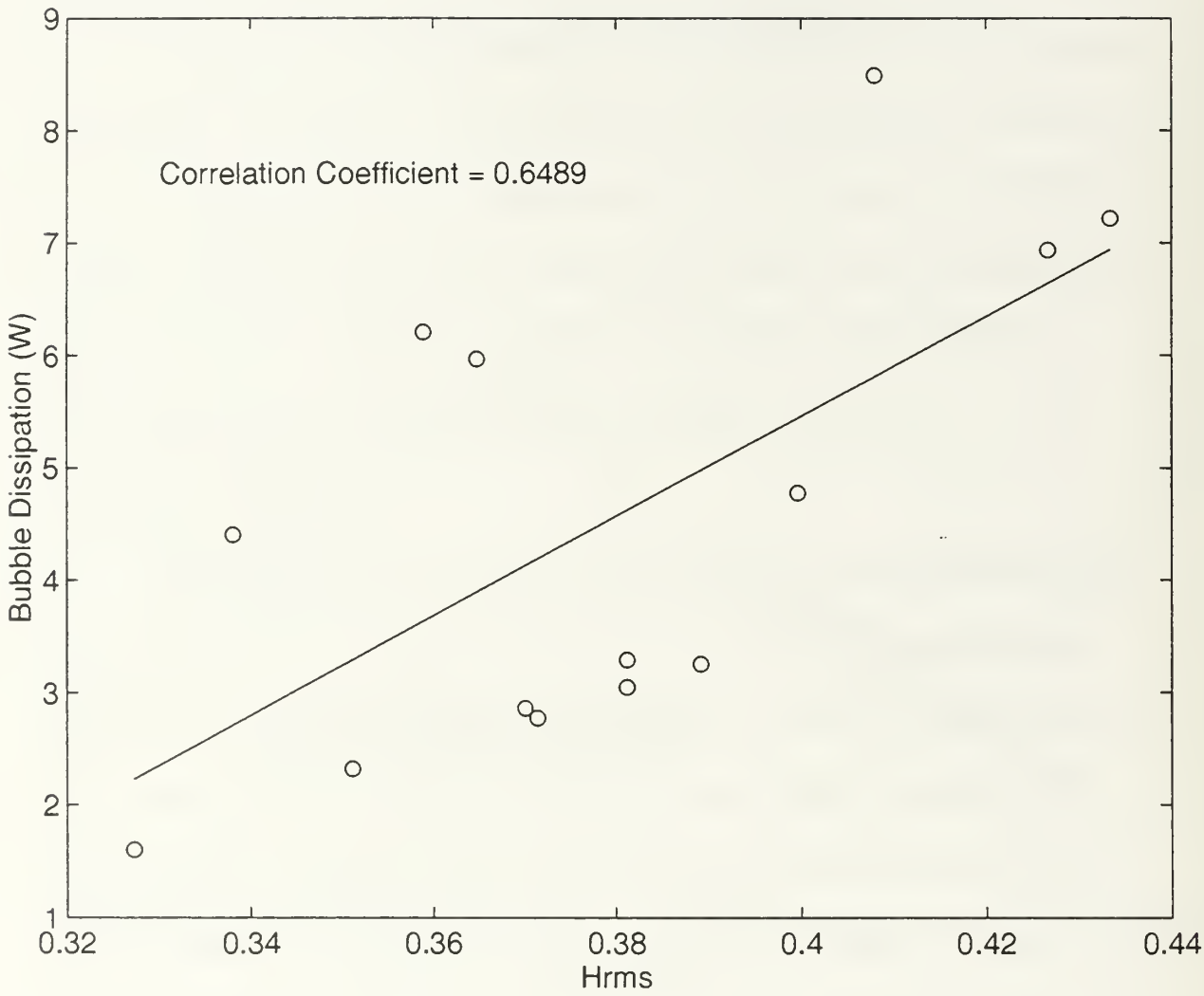

Figure 13. Bubble Dissipation vs. H_{rms}

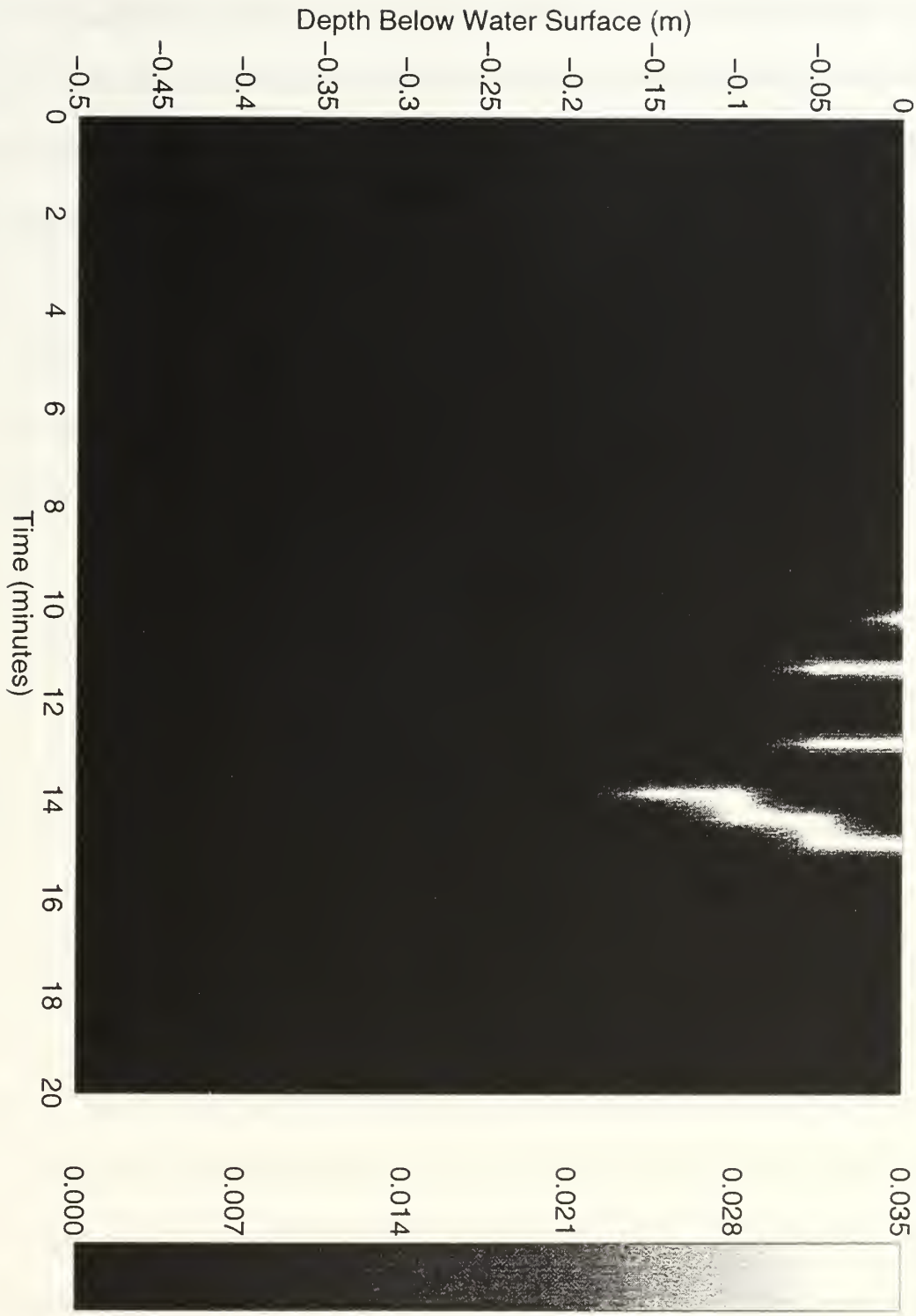

Figure 14. Void Fraction Distribution Below the Water Surface (η) vs. Time

measurements in the surf zone by Loewen and O'Dor. Percent of the Bubble Potential Energy dissipation rates to total wave dissipation in the cross shore direction is on the order of 8-20%. The potential energy dissipation is largest immediately after injection, decaying exponentially after that. The rate of energy dissipation in the vertical appears to be exponential. Bubble potential energy dissipated results within 1.2 seconds even for void fraction events greater than 36% and usually in less than 1.0 s. In this short time span, dissipation rates of greater than 200 Watts were observed. Energy dissipation is a function of wave height, since depth of injection is proportional to wave depth.

A conductivity array similar to the array used at the Monterey Bay Beach Experiment will be installed at DUCK 1997 in North Carolina. The length of data record will be longer, which will allow for more cases of wave breaking at the array. The array will be affixed to a moveable sled to observe breaking waves at various locations across the barred beach. The range of the wave heights should be larger for the two month experiment which will provide higher energy events with greater void fractions.

Future projects for this data include comparing the void fraction and bubble dissipation values with measured brightness levels digitized from the video data. The digitized values are available and a program to correlate the brightness levels with the position of the array already exists. Void fraction could be measured remotely if it could be related to relative brightness levels of the bore measured by video. Several remote video sites have been established

around the world which acquire surf zone video on a continuous or near continuous basis. The long time records due to increased stay time over waterborne measurement equipment and the relatively lower expense of video gear would mean more reliable data at a much cheaper cost.

LIST OF REFERENCES

Asher, W.E. and P.J. Farley, 1995, Phase-Doppler anemometer measurement of bubble concentrations in laboratory-simulated breaking waves, *J. Geophys. Res.,* **100**, 7045-7056.

Cartmill, J.W. and M.Y. Su, 1993, Bubble size distribution under saltwater and freshwater breaking waves, *Dynamics of Atmospheres and Oceans*, **20**, 25-31.

Fuhrboter, A., 1970, Air entrainment and energy dissipation in breakers, in *Proc. 12th Conf. on Coastal Eng.*, 391-398.

Gemmrich, J., 1992, Characteristics of breaking waves as observed by the drifter flex, in *Proc. First Intl. Symp. Ocean Wave Meas. and Anal.*, 963-974.

Haines, M.A. and B.D. Johnson, 1995, Injected bubble populations in seawater and fresh water measured by a photographic method, *J. Geophys. Res.*, **100**, 7057-7068.

Horikawa, K., and C. T. Kuo, 1966, A study of wave transformation inside surf zone, in *Proc. 4th Conf. on Coastal Eng.*, 217-233.

Hwung, H. H., J. M. Chyan and Y.C. Chung, 1992, Energy dissipation and air bubbles mixing inside surf zone, in *Proc. 23rd International Conf. on Coastal Eng.*, 308-321.

Jansen, P.C.M., 1986, Laboratory observations of the kinematics in the aerated region of breaking waves, *Coastal Eng.*, **9**, 453-477.

Lamarre, E. and W. Melville, 1991, Air entrainment and dissipation in breaking waves. *Nature*, **351**, 469-472.

Lamarre, E. and W. Melville, 1992, Instrumentation for measurement of void fraction in breaking waves: Laboratory and field results. *IEEE Journal of Ocean Engineering*, **17**, 204-215.

Lamarre, E. and W. Melville, 1994, Void-fraction measurements and sound-speed fields in bubble plumes generated by breaking waves. *J. Acoust. Soc. Am.*, **95**(3), 1317-1328.

Loewen, M.R., M. O'Dor and M. Skafel, 1996, Bubbles entrained by mechanically generated breaking waves. *J. Geophys. Res.*, **101**, 20759-769.

Maxwell, J.C., 1891, A treatise on electricity and magnetism. Dover, 314.

Medwin, H., and N. Breitz, 1989, Ambient and transient bubble spectral densities in quiescent seas and under spilling breakers, *J. Geophys. Res.*, **94**, 12,751-59.

Su, M.Y. and J. Cartmill, 1993, Breaking wave measurement by a void fraction technique, in *Proc. Second Intl. Symp. Ocean Wave Meas. and Anal.*, 951-962.

Thornton, E.B. and R. Guza, 1983, Transformation of wave height distribution, *J. Geophys. Res.*, **88**, 10, 5925-5938.

INITIAL DISTRIBUTION LIST

1. Defense Technical Information Center 2
   8725 John J. Kingman Road
   STE 0944
   Fort Belvoir, VA 22060-6218

2. Dudley Knox Library 2
   Naval Postgraduate School
   411 Dyer Rd.
   Monterey, CA 93943-5101

3. Chairman, Department of Oceanography..... 1
   Code OC/Bo
   Naval Postgraduate School
   Monterey, CA 93943

4. Dr. E.B. Thornton, Code Oc/Tm..... 2
   Oceanography Department
   Naval Postgraduate School
   Monterey, CA 93943-5121

5. Timothy P. Stanton..... 2
   Code OC/St
   Naval Postgraduate School
   Monterey, CA 93943

6. Prof. Thomas P. Lippmann..... 1
   Scripps Institute of Oceanography
   La Jolla, CA 92037

7. LT James B. Tannahill, USN..... 2
   388A Ricketts Road
   Monterey, CA 93940

8. Commander..... 1
   Naval Oceanography Command
   Stennis Space Center, MS 39529-5000

9. Library..... 1
   Scripps Institution of Oceanography
   University of California, San Diego
   La Jolla, CA 92093